Polarization dependence of x-ray absorption spectra in graphene

M. T. Chowdhury,[1] R. Saito,[1] and M. S. Dresselhaus[2]
[1]*Department of Physics, Tohoku University, Sendai 980-8578, Japan*
[2]*Department of Physics, Massachusetts Institute of Technology, Cambridge, Massachusetts 02139-4307, USA*
(Received 20 October 2011; published 9 March 2012)

We calculate the x-ray absorption spectra (XAS) for $1s$-π^* and $1s$-σ^* transitions in single layer graphene using the dipole approximation and we compare with experimental results. It is found that the in-plane and out-of-plane orientations of the dipole vectors, which correspond to the $1s$-π^* and $1s$-σ^* transitions, respectively, are responsible for the polarization dependence of the x-ray absorption intensity in graphene. Using the atomic matrix elements, the low-energy XAS peaks can be assigned.

DOI: 10.1103/PhysRevB.85.115410 PACS number(s): 78.70.Dm, 78.67.Wj

I. INTRODUCTION

Graphene is a two-dimensional (2D), single isolated atomic layer of graphite with sp^2 bonded carbon atoms. In this 2D sheet, carbon atoms are densely packed in a honeycomb lattice. Graphene is the main structural unit of graphite, carbon nanotubes, and fullerenes.[1] The band structure of 2D graphene was already known six decades ago,[2] but it has long been assumed that a purely two-dimensional single graphitic layer can never exist. However, in 2004, Novoselov *et al*. experimentally discovered a 2D graphene sheet using a simple method called micromechanical cleavage or the mechanical exfoliation technique.[3] Graphene is a promising material for future applications, for example, in spintronics and ultrafast photonics.[4,5]

X-ray absorption spectroscopy (XAS), photoemission spectroscopy, electron energy-loss spectroscopy are all very important methods for characterizing the electronic properties of materials.[6] In particular, XAS, which is a core electron excitation process, provides information not only about the core-electron energy, but also about the unoccupied electronic states in materials. When an x ray is incident on a material, the x-ray photons excite the core electrons, such as the $1s$ and $2s$ electrons to unoccupied states above the Fermi level. At a certain energy, the absorption increases drastically and gives rise to an absorption edge that occurs when the incident photon energy and the absorption edge energy are both matched to each other to cause the excitation of a $1s$ electron to the unoccupied states. Generally, if an electron is excited from the $1s$ ($2s$) orbital, the process is called K (L)-edge absorption. The XAS technique provides information about the density of states (DOS) of the unoccupied states since the DOS of the $1s$ energy band has a small bandwidth compared with that of the unoccupied electronic band.

Experimental observations of the x-ray absorption fine structure (XAFS) of graphite were done by many different groups.[7–11] Rosenberg *et al*. found important information regarding the angular dependence of the near-edge x-ray absorption fine-structure (NEXAFS) intensity for single-crystal graphite.[7] The NEXAFS spectra shows that the intensity changes as a function of the polarization angle α of light relative to the surface of graphene [see Fig. 3(c), discussed later in this paper]. At the same time, the final-state symmetry can be selected by varying α. That is to say, the intensity of the $1s$ to π^* (σ^*) transition is proportional to $\sin^2\alpha$ ($\cos^2\alpha$), which is important for characterizing the symmetry of the wave function. In this paper, we clarify the $\sin^2\alpha$ ($\cos^2\alpha$) dependence of the x-ray absorption intensity numerically and analytically by using a standard formalism within the dipole approximation. Apart from the well-known spectral features, such as the π^* and σ^* resonance peaks, Fischer *et al*. observed the so-called graphitic interlayer state at around 288 eV, which is not replicated in the unoccupied DOS.[8] Brühwiler *et al*. reported in studying the XAS spectra of highly oriented pyrolytic graphite (HOPG) that π^* and σ^* peaks have an excitonic nature and the spectral peak positions do not exactly correspond to the unoccupied DOS of graphite.[12] The excitonic nature of the XAS spectral peaks of graphite and diamond was also confirmed by Ma *et al*.[13]

Recently, several groups have experimentally observed the x-ray absorption spectra of a 2D monolayer and few layer graphene.[14–17] According to their observations, the peak at $\approx$285 eV is associated with a π^* transition, while the σ^* states appear at $\approx$292 eV. A sharp (weak) peak of the $1s$ to π^* (σ^*) transition is observed because the polarization direction was almost perpendicular to the basal plane of graphene, which is consistent with the results of Rosenberg *et al*.[7] mentioned above. There are two contributions to the XAS intensity: (1) the matrix element between the initial and final states, and (2) the joint density of states (JDOS) calculated from the energy-band structure. Such an enhancement or the absence of an enhancement of the transition intensity may be the effect of the polarization dependence of matrix elements. Pacilé *et al*.[14] observed a spectral feature at 288 eV in the carbon K-edge photoabsorption spectra of monolayer graphene, which they identified with an interlayer state. However, Jeong *et al*.[18] presented evidence against the existence of an interlayer state and concluded that the spectral feature at 288 eV originates from the COOH and/or C-H contamination at the surface of graphite. Zhou *et al*.[15] also showed the XAS spectra of single layer exfoliated graphene for two different polarizations. When the light polarization lies within the graphene basal plane, only the in-plane σ^* orbital contributes to the C $1s$ edge at 292 eV corresponding to the $1s$ to σ^* transition, while when the out-of-plane polarization component increases, the intensity of the π^* feature at 285 eV strongly increases. This polarization dependence confirms the in-plane and out-of-plane character, respectively, of the σ^* and π^* orbitals. Recently Hua *et al*.[19] calculated the XAS spectra for graphene using first-principles calculations. The infinite graphene sheet is here simulated

for different widths of graphene nanoribbons.[19] Using such a calculation, they analyzed the effect of edges, defects, or stacking order on the characteristics of the XAS spectra. An ideal 2D infinite graphene plane has one unique π^* peak. But in the case of real samples, due to the presence of edges, defects or broken periodic symmetry, additional features in the XAS can be created. From these spectral features, the interpretation of the XAS spectra of graphene can be made under the different conditions. In this context, the unoccupied electronic structure of nanographene in pristine and fluorinated activated carbon fibers (ACF) was investigated with NEXAFS by Kiguchi *et al.*[20] Apart from the two prominent spectral features π^* at 285.5 eV and σ^* at 291.9 eV, two extra peaks were formed and were attributed to the edge states at 284.5 eV, which is very close to the Fermi level at 284.4 eV of HOPG and at 284.9 eV corresponds to the dangling bond states originating from fluorination. A new peak that is identified with the σ^* peak appeared at 290 eV below the characteristic σ^* peak. This peak appears as a consequence of the C-F bond at the expense of the π bond. The presence of the edge state in a graphene nanoribbon was observed by Joly *et al.*[21] using NEXAFS. They also reported that as the annealing temperature increases, the intensity of the edge state decreases. Therefore x-ray absorption spectroscopy is very useful for the characterization of graphene.

Grüneis *et al.*[22] explained the optical-absorption spectra that correspond to π-π^* transitions for graphene and carbon nanotubes within the dipole approximation in which the absorption amplitude is proportional to the inner product of the polarization vector $\vec{P}$ and the dipole vector $\vec{D}$ (i.e., as $\vec{P}\cdot\vec{D}$). The π-π^* interband transition process is assumed to be a vertical transition where the photon momentum is negligible compared to the typical size of the Brillouin zone. Grüneis *et al.*[22] show that an analytic interpretation of the optical absorption process in 2D reciprocal space can give us important information which cannot be obtained directly from the energy-dependent optical-absorption spectra without such an analysis. Such an analytical description for the x-ray absorption process has not been available until now. The objective of this paper is to formulate an analytical picture that can explain the polarization dependence of the x-ray absorption spectra of graphene.

This paper is organized as follows. In Sec. II A we describe the formulation of the x-ray absorption spectra of graphene using the dipole approximation. The initial and the final states are expressed as a summation of the Bloch functions. The so-called dipole approximation is reviewed in this section following the previous work of Grüneis *et al.*[22] However, it is noted that the dipole approximation for the x-ray absorption process cannot be treated as a vertical transition in k space. In this content, atomic matrix elements for the on-site and off-site transitions are discussed in this paper in which the expression for the on-site and the off-site matrix elements are analytically formulated for XAS. We define the JDOS (joint density of states) in this section because it corresponds to the x-ray absorption spectra. In Sec. II B, we discuss how the atomic orbitals are fitted to a sum of Gaussian functions. We then summarize the fitting parameters for the $1s$, $2s$, and $2p$ atomic orbitals and using the fitting parameters, obtained by this analytic procedure, the on-site and off-site atomic matrix elements are calculated. Thus the x-ray absorption intensity for the $1s$-π^* and $1s$-σ^* transitions is explained by analyzing the dipole vector and oscillator strength as a function of the final wave vectors. In Sec. III, the calculated XAS spectra are discussed in the light of the JDOS and the results of our calculated XAS spectra are compared to the experimental results reported previously as described above. A conclusion is given in Sec. IV.

II. X-RAY ABSORPTION SPECTRA

A. Calculation method

In Fig. 1(a) the calculated energy dispersion relations of graphene for the π and σ bands are shown, as here calculated within the simple tight-binding method as summarized below. The tight-binding parameters used to calculate the energy dispersion are obtained from the published calculations by R. Saito *et al.*[1] To calculate the energy dispersion of the $1s$ band of graphene which is shown in Fig. 1(b), we have assumed the nearest-neighbor transfer integral, $t = -0.1$ eV and the overlap integral $s = 0.0$. The calculated energy bandwidth of the $1s$ band is 0.3 eV, which is almost flat compared with that of the π and σ bands. The matrix element for the photoabsorption process within the dipole approximation is expressed by Grüneis *et al.*[22] as

$$M_{\rm opt}^{fi}(\vec{k}_f,\vec{k}_i) = \langle \Psi^f(\vec{k}_f) \mid H_{\rm opt} \mid \Psi(\vec{k}_i)\rangle = \vec{P}\cdot\vec{D}^{fi}(\vec{k}_f,\vec{k}_i),$$

where "i" ($\vec{k}_i$) and "f" ($\vec{k}_f$) stand for the initial and final states (wave vectors), respectively. In the case of the x-ray absorption process, the initial state is a $1s$ energy band and the final state is either a π^* or σ^* unoccupied energy band. Here $H_{\rm opt}$ denotes a perturbation Hamiltonian for the optical dipole transition.

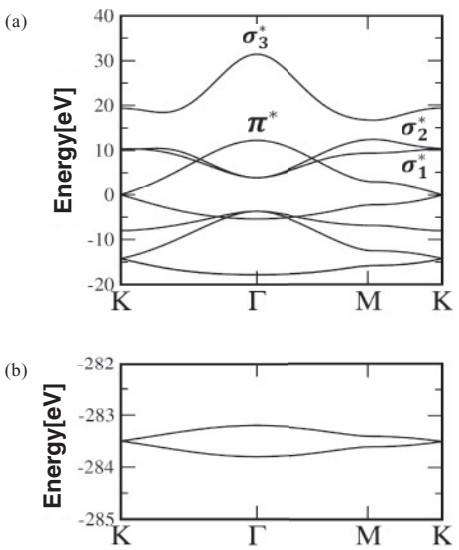

FIG. 1. (a) The calculated energy dispersion relations of the π and σ bands of 2D graphene along various high-symmetry directions. (b) The calculated energy dispersion relations of the $1s$ bands of 2D graphene along various high-symmetry directions.

$\vec{P}$ is the polarization vector of the light, and the matrix element $\vec{D}^{fi}(\vec{k}_f,\vec{k}_i)$ for the dipole vector is defined as

$$\vec{D}^{fi}(\vec{k}_f,\vec{k}_i) = \langle \Psi^f(\vec{k}_f) \mid \nabla \mid \Psi(\vec{k}_i)\rangle. \tag{1}$$

The wave function for the initial ($1s$) and the final states (π^*, σ^*) can be expressed by

$$\Psi^{1s}(\vec{k}) = C_A^{1s}(\vec{k})\Phi_A^{1s}(\vec{k},\vec{r}) + C_B^{1s}(\vec{k})\Phi_B^{1s}(\vec{k},\vec{r}), \tag{2}$$

$$\Psi^{2p_z}(\vec{k}) = C_A^{2p_z}(\vec{k})\Phi_A^{2p_z}(\vec{k},\vec{r}) + C_B^{2p_z}(\vec{k})\Phi_B^{2p_z}(\vec{k},\vec{r}), \tag{3}$$

so that the wave function for the σ band is written as

$$\begin{aligned}\Psi^{\sigma}(\vec{k}) = {} & C_A^{2s}(\vec{k})\Phi_A^{2s}(\vec{k},\vec{r}) + C_A^{2p_x}(\vec{k})\Phi_A^{2p_x}(\vec{k},\vec{r}) \\ & + C_A^{2p_y}(\vec{k})\Phi_A^{2p_y}(\vec{k},\vec{r}) + C_B^{2s}(\vec{k})\Phi_B^{2s}(\vec{k},\vec{r}) \\ & + C_B^{2p_x}(\vec{k})\Phi_B^{2p_x}(\vec{k},\vec{r}) + C_B^{2p_y}(\vec{k})\Phi_B^{2p_y}(\vec{k},\vec{r}),\end{aligned} \tag{4}$$

where the unit cell of graphene consists of two atoms A and B. In the above equations, Φ_A and Φ_B are the Bloch functions for the $1s$, $2s$, $2p_z$, $2p_x$, $2p_y$ atomic orbitals on A and B sites. The Bloch function $\Phi(\vec{k},\vec{r})$ can be written as a summation of atomic orbitals φ at the position of the indicated atoms $\vec{R}$,

$$\Phi(\vec{k},\vec{r}) = \frac{1}{\sqrt{N}}\sum_{\vec{R}} \exp[-i\vec{k}\cdot\vec{R}]\varphi(\vec{r}-\vec{R}), \tag{5}$$

where N denotes the number of unit cells in the crystal. When we are considering the vector $\vec{D}^{fi}$ in Eq. (1) for only the nearest-neighbor atoms, $\varphi(\vec{r}-\vec{R})$ of the initial and final states can be either the same atom (on site) or one of the nearest-neighbor atoms (off-site) when using three wave functions for constructing matrix elements.[22] The on-site and the off-site atomic dipole vectors for a $1s$ to π^* transition can be defined as

$$\vec{D}^{\rm on}(\vec{k}_f,\vec{k}_i) = C_A^{f^*}(\vec{k}_f)C_A^{i}(\vec{k}_i)m_{\rm opt}^{AA}\hat{\vec{z}} + C_B^{f^*}(\vec{k}_f)C_B^{i}(\vec{k}_i)m_{\rm opt}^{BB}\hat{\vec{z}}, \tag{6}$$

and

$$\begin{aligned}\vec{D}^{\rm off}(\vec{k}_f,\vec{k}_i) = {} & C_A^{f^*}(\vec{k}_f)C_B^{i}(\vec{k}_i)\sum_{l=1}^{3}\exp\big(-i\vec{r}_A^{\,l}\cdot\vec{k}_f\big)m_{\rm opt}^{AB}\hat{\vec{z}} \\ & + C_B^{f^*}(\vec{k}_f)C_A^{i}(\vec{k}_i)\sum_{l=1}^{3}\exp\big(-i\vec{r}_B^{\,l}\cdot\vec{k}_f\big)m_{\rm opt}^{BA}\hat{\vec{z}},\end{aligned} \tag{7}$$

where $m_{\rm opt}^{AA}$ ($m_{\rm opt}^{BB}$) and $m_{\rm opt}^{AB}(m_{\rm opt}^{BA})$ are the on-site and off-site atomic matrix elements, respectively. Hereafter we denote $m_{\rm opt}^{AA} = m_{\rm opt}^{BB}$ as $m_{\rm opt}^{\rm on}$ and $m_{\rm opt}^{AB} = m_{\rm opt}^{BA}$ as $m_{\rm opt}^{\rm off}$. Then for a $1s$ to π^* transition, the on-site and off-site atomic matrix elements can be expressed, respectively, as

$$m_{\rm opt}^{\rm on} = \langle\varphi^{2p_z}(\vec{r}) \mid \frac{\delta}{\delta z} \mid \varphi^{1s}(\vec{r})\rangle, \tag{8}$$

and

$$m_{\rm opt}^{\rm off} = \langle\varphi^{2p_z}(\vec{r}-\vec{r}_l) \mid \frac{\delta}{\delta z} \mid \varphi^{1s}(\vec{r})\rangle. \tag{9}$$

For the $1s$ to σ^* transition, the x-ray absorption for both the on-site and off-site interactions has a nonzero value for the dipole vector in the x and y directions because of the mirror symmetry of the graphene plane. We can express the dipole vector for the $1s$ to σ^* transition in terms of an off-site and on-site interaction. Thus the dipole vector $\vec{D}(\vec{k}_f,\vec{k}_i)$ can be written as

$$\begin{aligned}\vec{D}(\vec{k}_f,\vec{k}_i) = {} & \sum_{m,n=A,B}\ \sum_{o=2s,2p_x,2p_y;o'=1s} C_m^{o^*}(\vec{k}_f)C_n^{o'}(\vec{k}_i) \\ & \times\big\langle\Phi_m^{o}(\vec{k}_f,\vec{r})\big|\nabla\big|\Phi_n^{o'}(\vec{k}_i,\vec{r})\big\rangle,\end{aligned} \tag{10}$$

where the summation on m and n is taken over A or B and the summation on o (o') is taken over $2s$, $2p_x$, $2p_y$ ($1s$ orbital) orbitals. We can decompose $\vec{D}(\vec{k}_f,\vec{k}_i)$ into an on-site $\vec{D}^{\rm on}(\vec{k}_f,\vec{k}_i)$ and an off-site $\vec{D}^{\rm off}(\vec{k}_f,\vec{k}_i)$ component as follows:

$$\begin{aligned}\vec{D}^{\rm on}(\vec{k}_f,\vec{k}_i) = {} & \sum_{n=A,B}\ \sum_{o=2s,2p_x,2p_y;o'=1s} C_n^{o^*}(\vec{k}_f)C_n^{o'}(\vec{k}_i) \\ & \times\big\langle\Phi_n^{o}(\vec{k}_f,\vec{r})\big|\nabla\big|\Phi_n^{o'}(\vec{k}_i,\vec{r})\big\rangle,\end{aligned} \tag{11}$$

and

$$\begin{aligned}\vec{D}^{\rm off}(\vec{k}_f,\vec{k}_i) = {} & \sum_{m\neq n=A,B}\ \sum_{o=2s,2p_x,2p_y;o'=1s} C_m^{o^*}(\vec{k}_f)C_n^{o'}(\vec{k}_i) \\ & \times\big\langle\Phi_m^{o}(\vec{k}_f,\vec{r})\big|\nabla\big|\Phi_n^{o'}(\vec{k}_i,\vec{r})\big\rangle,\end{aligned} \tag{12}$$

respectively. The on-site and off-site atomic matrix elements for the $1s$ to σ^* transition can be defined as

$$\begin{aligned}m_{\rm opt}^{\rm on} &= \langle\varphi^{2p_x}(\vec{r}) \mid \frac{\delta}{\delta x} \mid \varphi^{1s}(\vec{r})\rangle \\ &= \langle\varphi^{2p_y}(\vec{r}) \mid \frac{\delta}{\delta y} \mid \varphi^{1s}(\vec{r})\rangle,\end{aligned} \tag{13}$$

$$\begin{aligned}m_{\rm opt}^{\rm off} &= \langle\varphi^{2p_x}(\vec{r}-\vec{r}_l) \mid \frac{\delta}{\delta x} \mid \varphi^{1s}(\vec{r})\rangle \\ &= \langle\varphi^{2p_y}(\vec{r}-\vec{r}_l) \mid \frac{\delta}{\delta y} \mid \varphi^{1s}(\vec{r})\rangle,\end{aligned} \tag{14}$$

and

$$m_{\rm opt}^{\rm off,S} = \langle\varphi^{2s}(\vec{r}-\vec{r}_l) \mid \frac{\delta}{\delta x} \mid \varphi^{1s}(\vec{r})\rangle, \tag{15}$$

where $\vec{r}_l$ is the vector that connects the first nearest-neighbor atom in the direction of the x axis.

In the x-ray absorption process, the photon momentum is not negligible compared with the electron momentum in the 2D Brillouin zone, once the considerations of the photon momentum give rise to a nonvertical transition. Thus energy-momentum conservation for an electron gives the following equations:

$$E_f(\vec{k}_f) - E_i(\vec{k}_i) = E_l, \tag{16}$$

$$\vec{k}_i + \vec{k}_l = \vec{k}_f, \tag{17}$$

$$E_l = \hbar\omega = \hbar c\vec{k}_l, \tag{18}$$

where $\vec{k}_i$, $\vec{k}_f$, and $\vec{k}_l$ are the initial, final momentum of the electron, and the photon momentum of the incident light photon. Here $E_i(\vec{k}_i)$ and $E_f(\vec{k}_f)$ are, respectively, the energy of the electron in the initial and in the final state as a function of the initial and final electron momentum $\vec{k}_i$ and $\vec{k}_f$. In the above equations, E_l is the incident light energy around 284 eV, c is the speed of light in vacuum, and $\hbar$ is the Planck constant/2π.

The corresponding photon momentum $\vec{k}_l$ is $\sim 10^9$/m, which corresponds to about 10% of the typical size of the Brillouin zone (10^{10}/m), and wave vectors of this magnitude cannot be neglected. Hence the x-ray absorption process is not a vertical transition, and therefore many final states with different $\vec{k}_f$ appear for each $\vec{k}_i$, which is an essential point for discussing the physics of the XAS process.

Fermi's "golden rule" is used to calculate the transition probability from $\vec{k}_i$ to $\vec{k}_f$. Within the dipole approximation,[22] the XAS intensity I as a function for E_l of $\vec{k}_i$ and $\vec{k}_f$ is given by

$$I(E_l) \propto \iint |\vec{P} \cdot \vec{D}^{fi}(\vec{k}_f, \vec{k}_i)|^2 \delta[E(\vec{k}_f) - E(\vec{k}_i) - E_l] d\vec{k}_f d\vec{k}_i, \tag{19}$$

where the integration is taken over the entire 2D Brillouin zone. Here $\vec{k}_f$ can be selected by the energy-momentum conservation for nonvertical transitions, which is shown by the terms within the δ function in Eq. (19). Integration of the δ function in Eq. (19) gives the normalizatons for the intensity in spite of the $|\vec{P} \cdot \vec{D}^{fi}|^2$ term, which contributes over the entire 2D Brillouin zone to give the joint density of states (JDOS), which is written as

$$\mathrm{JDOS}(E_l) = \iint \delta[E(\vec{k}_f) - E(\vec{k}_i) - E_l] d\vec{k}_f d\vec{k}_i. \tag{20}$$

B. Atomic orbitals

An atomic orbital can be expressed as a summation of Gaussian functions with coefficients I_k and a corresponding Gaussian width σ_k. Using a nonlinear fitting method, we can fit such Gaussian functions to *ab initio* calculated wave functions to obtain the fitting parameters I_k and σ_k, $(k = 1, \ldots, n)$. Here the *ab initio* calculation refers to the atomic Schrödinger equation that was used to obtain atomic orbitals for the carbon atoms in previous work.[23,24]

The functional form of the Gaussian used for the $2p_z$ atomic orbital can be expressed as

$$\varphi(r) = z \frac{1}{\sqrt{N_t}} \sum_{k=1}^{n} I_k \exp\left\{\frac{-r^2}{2\sigma_k^2}\right\}, \tag{21}$$

where z denotes the angular part of the orbital wave function. N_t, I_k, and σ_k are, respectively, the normalization constant, coefficient, and width of the Gaussian. Here t is the index for an atomic orbital, i.e., $t = 1s, 2s, 2p$.

The radial part of the atomic orbital ($1s$, $2s$, $2p$) can be expressed as

$$f^t(r) = \sum_{k=1}^{n} I_k^t \exp\left\{\frac{-r^2}{2(\sigma_k^t)^2}\right\}. \tag{22}$$

The same functional form of Eq. (22) can be chosen for the $1s$ and $2s$ atomic orbitals even though the $2s$ orbitals have a node in the direction of r. The normalization constant for the $2p$ ($2p_x$, $2p_y$, and $2p_z$) orbitals can be given by

$$N_{2p} = \frac{\sqrt{8\pi^3}}{3} \sum_{l=1,k=1}^{n} I_k I_l \left(\frac{1}{\sigma_k^2} + \frac{1}{\sigma_l^2}\right)^{-3/2}. \tag{23}$$

TABLE I. Fitting parameters for the $1s$, $2s$, and $2p$ orbitals.

m	n	1	2	3	4
	I_k	7.75130	11.61669	6.04298	1.92502
$1s$	σ_k	0.28740	0.11206	0.03510	0.00665
	I_k	−0.95773	2.75838	0.94915	3.53458
$2s$	σ_k	1.36189	0.07458	0.01434	0.23196
	I_k	0.25145	0.76498	−0.67498	3.53458
$2p$	σ_k	2.25320	1.03192	0.14805	0.02893

The normalization constant used for the $1s$ and $2s$ orbitals can be given by

$$N_s = \sqrt{8\pi^3} \sum_{l=1,k=1}^{n} I_k I_l \left(\frac{1}{\sigma_k^2} + \frac{1}{\sigma_l^2}\right)^{-3/2}. \tag{24}$$

In summary, the fitting parameters for the $1s$, $2s$, and $2p$ orbitals are given in Table I.

The atomic matrix element $m_{\mathrm{opt}}^{\mathrm{on}}$ for the $1s$ to π^* on-site transition is then calculated analytically by Gaussian functions and we get $m_{\mathrm{opt}}^{\mathrm{on}} = 0.30(\mathrm{a.u.})^{-1}$, and the dipole vector related to this matrix element is an even function of z. Here $1(\mathrm{a.u.}) = 0.529$ Å. For the $1s$ to σ^* on-site transition, we get a matrix element from two in-plane orbitals, $2p_x$ and $2p_y$. The atomic matrix elements due to these $1s$ to σ^* transitions are $0.30(\mathrm{a.u.})^{-1}$, which is the same as for the $1s$ to π^* transition. Because of the orbital symmetry of the $2p_x$ and $2p_y$ orbitals, the dipole vector for the $1s$ to σ^* on-site transition lies in the direction of the xy graphene basal plane. Although the $2s$ orbital contributes to the σ orbital, the $2s$ orbital does not contribute to the on-site transition because the matrix element $\langle 2s \mid \nabla \mid 1s \rangle$ is an odd function of x, y, or z and is thus zero by symmetry. The atomic matrix element for the $1s$ to π^* off-site transition has a value of $5.2 \times 10^{-2}[\mathrm{a.u}]^{-1}$. We have also calculated the $1s$ to $2s$ off-site atomic matrix element which is $-6.96 \times 10^{-2}(\mathrm{a.u.})^{-1}$. The negative sign appears because there is a node in the radial wave function of the $2s$ orbital. Since the distance between the C-C atom is 2.71 a.u., the wave function of the $1s$ orbital of the carbon atom quickly decreases with increasing distance. Thus the overlap between the $1s$ and $2p$ orbitals ($2p_x, 2p_y, 2p_z$) is much weaker than that of the π to π^* transition reported by Grüneis *et al.* $[0.21(\mathrm{a.u})^{-1}]$.[22] The calculated results for the atomic matrix element can be summarized in Table II. By analyzing the atomic matrix element, the direction of the dipole vector is given by the atomic dipole vector, which is independent of the wave vector k. The k-dependent part appears within the wave function coefficient in the case of the on-site interaction and the wave function coefficient, and within the phase factor in the case of the off-site interaction.

In Fig. 2 the joint density of states (JDOS) for the $1s$ to π^* and the $1s$ to σ_j^* $(j = 1, \ldots, 3)$ transitions for 2D graphene are shown. The peak around 286.4 eV in Fig. 2 corresponds to the $1s$-π^* transition peak and the peak around 293.4 eV corresponds to the so-called $1s$-σ^* transition peak, which has contributions mainly coming from the σ_1^* and σ_2^* bands shown in Fig. 1(a). The third peak at around 302.5 eV originates mainly from contributions from the σ_3^* band, also shown in Fig. 1(a).

TABLE II. Atomic matrix element m_{opt} for the on-site and off-site transitions. $\vec{r}$ is the direction of the nearest neighbor.

Transition	$m_{\text{opt}}^{\text{on}}$ [(a.u.)$^{-1}$]	Direction	$m_{\text{opt}}^{\text{off}}$ [(a.u.)$^{-1}$]
$1s$-$2p_z$	0.303	z	5.274×10^{-2}
$1s$-$2s$	0.000	$\vec{r}$	-6.961×10^{-2}
$1s$-$2p_x$	0.303	x	5.274×10^{-2}
$1s$-$2p_y$	0.303	y	5.274×10^{-2}
$2p_z$-$2p_z$ (Ref. 22)	0.000	$\vec{r}$	0.210

Now let us consider the x-ray absorption intensity for the $1s$-π^* transition. The incident energy is chosen as 286.4 eV because we found from the JDOS in Fig. 2 that the $1s$-π^* transition occurs at 286.4 eV. In Figs. 3(a) and 3(b) we plot the oscillator strength and the x-ray absorption intensity for the $1s$-π^* transition as a function of the final wave vector k_f in the 2D Brillouin zone, respectively. The oscillator strength[22] is defined as the inner product of the dipole vector, i.e., $\sqrt{\vec{D} \cdot \vec{D}}$. Even though the oscillator strengths around the K point and the M point are very small, they are nevertheless not zero and thus we can get strong x-ray absorption around the K points because many final-state k_f points satisfy energy-momentum conservation along M-M lines in the Brillouin zone. The oscillator strength is found to be a maximum at the Γ point but the absorption intensity is found to be zero at the Γ point because no k_f points exist at or near the Γ point that satisfy the energy-momentum conservation requirements. That is, the multiplication between the δ function and the square of the matrix element of Eq. (19) gives the intensity distribution in the 2D Brillouin zone. The dipole vector for the $1s$ to σ^* transition is the summation of the atomic dipole vectors for the $1s$ to $2s$, $2p_x$, and $2p_y$ orbitals. Because x, y, and z are all odd functions, the dipole vector for the $1s$ to $2s$ on-site transition vanishes. Then the $1s$ to σ^* on-site transition only consists of the $1s$ to $2p_y$ and the $1s$ to $2p_x$ transitions. The dipole vector lies along the x or y direction if the final states are $2p_x$ or $2p_y$ orbitals, respectively. Let us plot the dipole vector for the transition from the $1s$ to the two unoccupied lower energy σ^* bands, which we denote as σ_1^* and σ_2^*. The

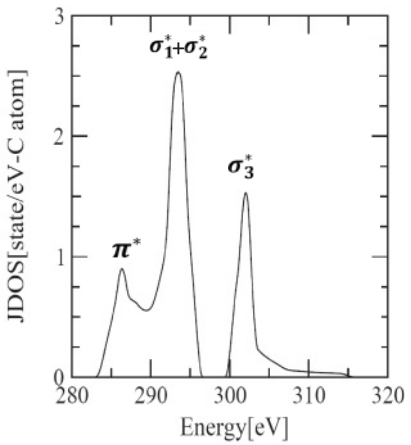

FIG. 2. The joint density of states (JDOS) of graphene as a function of energy. The JDOS is calculated from the occupied $1s$ orbitals to unoccupied states.

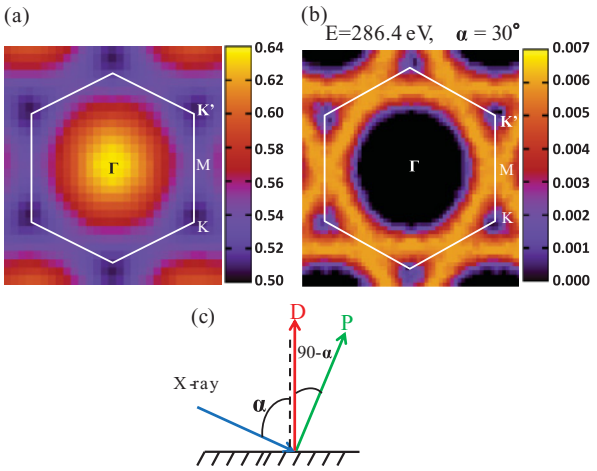

FIG. 3. (Color online) (a) The oscillator strength for the $1s$ to π^* transition as a function of the final wave vector $\vec{k}_f$ in the 2D Brillouin zone. The bright (dark) area shows the strong (weak) oscillator strength. The numbers in the color bar are given in the units of $m_{\text{opt}}^{\text{on}}$. (b) The x-ray absorption intensity [the bright (dark) area shows strong (weak) x-ray absorption] of the $1s$ to π^* transition as a function of the final wave vector $\vec{k}_f$ in the 2D Brillouin zone of graphene. Here we use the x-ray energy $E = 286.4$ eV and $\alpha = 30^\circ$. The units of the x-ray absorption intensity are (a.u.)$^{-2}$ as shown in the color bars. (c) The polarization angle α is defined by the angle between the propagating direction of the x-ray and the dipole vector D, which is perpendicular to the graphene basal plane. P is the polarization direction of the x-ray light.

on-site dipole vectors for the $1s$ to σ_1^* and to σ_2^* transitions are shown in Figs. 4(a) and 4(b), respectively. If we closely look at Figs. 4(a) and 4(b), respectively, we observe that the on-site dipole vectors near the Γ point for the $1s$ to σ_1^* and σ_2^* transition are in radial and tangential directions, respectively. On the other hand, near the $K(K')$ point, the on-site dipole vector for the $1s$ to σ_1^* and σ_2^* transition are directed, respectively, in the tangential and radial directions, which is an opposite behavior to that near the Γ point.

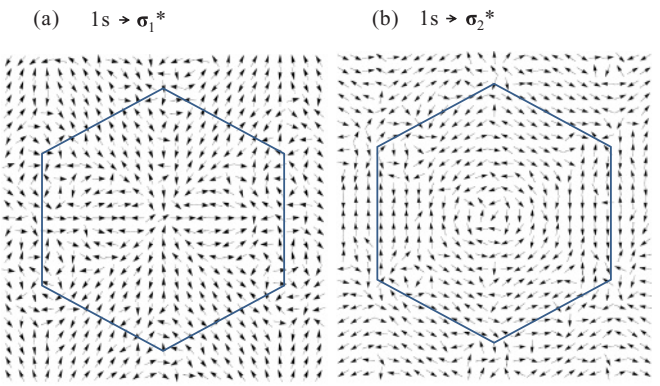

FIG. 4. (Color online) On-site normalized dipole vectors for (a) the $1s$ to σ_1^* transition and (b) the $1s$ to σ_2^* transition as a function of the final wave vector $\vec{k}_f$ in the 2D Brillouin zone.

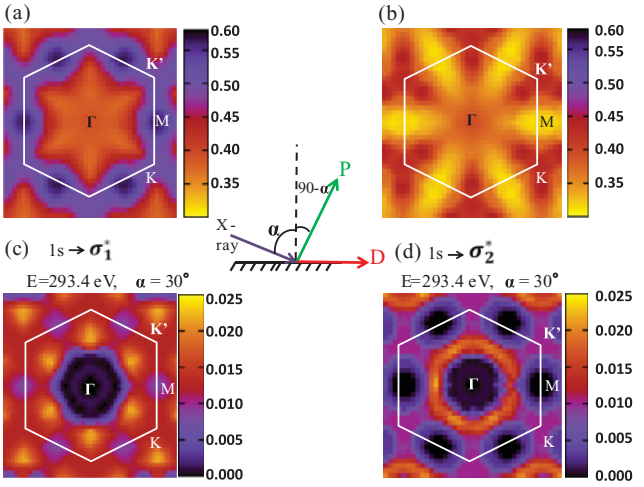

FIG. 5. (Color online) The oscillator strength (a) for the $1s$ to σ_1^* on-site transition and (b) for $1s$ to σ_2^* on-site transition. The bright (dark) area shows as strong (weak) oscillator strength. The numbers in the color bar are given in units of $m_{\rm opt}^{\rm on}$. Here we use the value of the on-site atomic matrix element as $m_{\rm opt}^{\rm on} = 0.30$(a.u.)$^{-1}$. The x-ray absorption intensity [the bright (dark) area shows strong (weak) x-ray absorption] of (c) the $1s$ to σ_1^* transition and (d) the $1s$ to σ_2^* transition as a function of the final wave vector $\vec{k}_f$ in the 2D Brillouin zone of graphene for the x-ray energy $E = 293.4$ eV and $\alpha = 30^\circ$. The direction of the polarization vector P and the direction of the dipole vector D for the $1s$ to σ^* transition, which acts along the xy graphene basal plane, are shown. The units of the x-ray absorption intensity shown in the color bars are (a.u.)$^{-2}$.

Now let us recall the dipole vector for the $1s$ to σ^* on-site transition, which can be written as

$$\vec{D}^{\rm on}(\vec{k}_f,\vec{k}_i) = C_A^{2p_x^*}(\vec{k}_f)C_A^{1s}(\vec{k}_i)m_{\rm opt}^{AA}\hat{\vec{x}} + C_A^{2p_y^*}(\vec{k}_f)C_A^{1s}(\vec{k}_i)m_{\rm opt}^{AA}\hat{\vec{y}}. \quad (25)$$

According to Eq. (25), the direction of the dipole vectors in the 2D Brillouin zone give us information about the symmetry of the corresponding final states, which are given by the wave function coefficients $C_A^{2p_x^*}(\vec{k}_f)$ and $C_A^{2p_y^*}(\vec{k}_f)$. It is noted that the dipole vectors for σ_1^* and σ_2^* are perpendicular to each other, as shown in Figs. 4(a) and 4(b), respectively, where the lower energy antibonding states have a distinct symmetry that shows the atomic orbital nature of the final states.

In Figs. 5(a) and 5(b), respectively we plot the oscillator strength for the $1s$-σ_1^* and $1s$-σ_2^* transitions as a function of the final wave vector k_f in the 2D Brillouin zone. For the $1s$ -σ_1^* transition, the oscillator strength becomes a maximum near the Γ point and a minimum near the M points but that minimum is not zero. On the other hand, for the $1s$-σ_2^* transition, shown in Fig. 5(b), the oscillator strength is a maximum at the M points and a minimum around the K points. Figures 5(c) and 5(d) show the x-ray absorption intensity as a function of k_f for the $1s$-σ_1^* and $1s$-σ_2^* transitions, respectively, at an energy of 293.4 eV and an angle of $\alpha = 30^\circ$. In spite of the moderate oscillator strength, the x-ray absorption intensity is found to be zero around the Γ point due to the symmetry, as mentioned above.

III. XAS AND THE JOINT DENSITY OF STATES (JDOS)

If we want to compare the calculated JDOS with the experimental XAS spectra, we must take into account the angle dependent matrix element, which is responsible for the polarization dependence of the XAS spectra. As, for example, at $\alpha = 0^\circ$ or at $\alpha = 90^\circ$, only the σ or π JDOS will appear in the XAS spectra, respectively.

In Figs. 6(a) and 6(b), we plot the experimental XAS spectra and the calculated XAS spectra, respectively, for various values of the polarization angle α. Figures 7(a) and 7(b) show that the relative peak intensity of peak A, denoted by the dashed line A (for the $1s$-π^* transition) and peak B, denoted by the solid line B (for the $1s$-σ^* transition) shown in Fig. 6(b) are linearly proportional to $\sin^2\alpha$ and $\cos^2\alpha$, respectively, which is consistent with the results given by Rosenberg *et al.*[7] The α dependence appears because the x-ray absorption intensity is proportional to the square of the absorption matrix element, i.e., $|\vec{P}\cdot\vec{D}|^2$. In the energy between 286.7 and 296.0 eV in Fig. 6(b), the calculated x-ray absorption intensity has contributions from both the π and σ bands. This overlapping of XAS contributions is not only dependent on the energy-dependent JDOS but also depends on the angle dependent matrix elements $\vec{P}\cdot\vec{D}$. We have compared our calculated XAS spectra with the experimental XAS spectra at different angles α and the results are shown in Fig. 6. Two prominent peaks found at 286.4 and 293.4 eV are obtained from our calculated XAS spectra by the dashed line A and solid line B peaks, respectively, which are denoted by their π^* and σ^* symmetry, respectively, as shown in Fig. 6(b). The

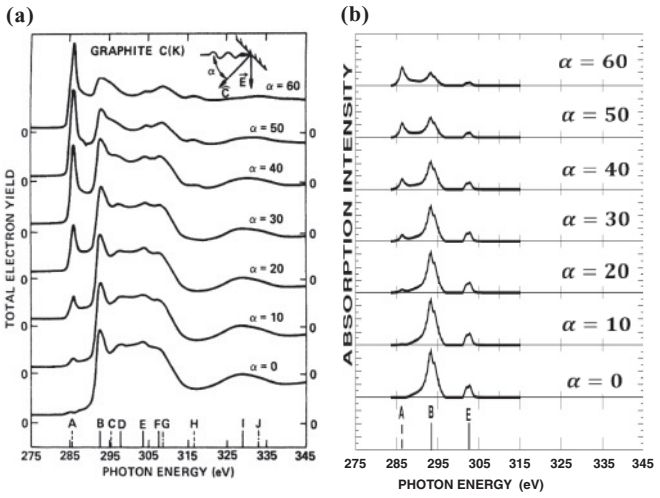

FIG. 6. (a) The C(K)-edge absorption spectra of single-crystal graphite at various polarization angles α between the surface normal and the Poynting vector of the light. Short lines with labels from A to J at the bottom of the figure are lines that denote the peak energies of various spectral features: dashed lines represent the states of π^* symmetry, while solid lines represent the states of σ^* symmetry. States whose symmetry could not be determined are represented by dashed dotted lines. The monochromatic photon energy calibration is estimated to be accurate to ± 0.5 eV (reproduced from Fig. 1 of Ref. 7); (b) the calculated XAS spectra of graphene. The dashed (solid) lines at the bottom show the contribution from the π^* (σ^*) orbitals.

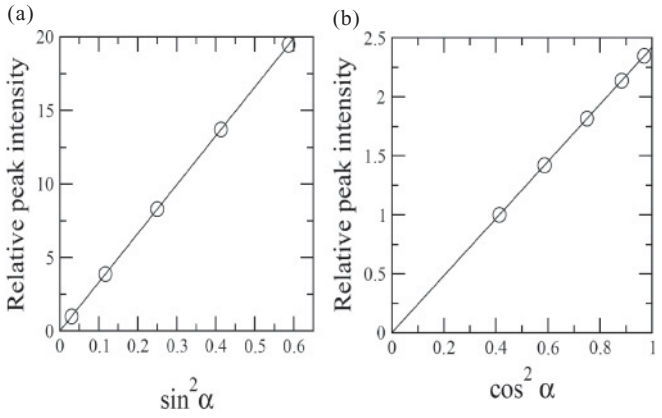

FIG. 7. (a) Relative peak intensities for the 1s to π^* transitions as a function of $\sin^2\alpha$. (b) Relative peak intensities for the 1s to σ^* transitions as a function of $\cos^2\alpha$. The circles are calculated results the lines are a guide to the eye.

corresponding experimental peaks for the 1s to π^* and 1s to σ^* transitions were observed at 285.5 eV (dashed line A) and 292.5 eV (solid line B), respectively, as shown in Fig. 6(a). The calculated results show a reasonable agreement with the experimentally observed spectra except for the peak positions, which are found to be slightly higher than those in the experiment. In this calculation, we use a single-particle DOS to calculate the x-ray absorption intensity. Thus such a difference between the calculated value and the observed value[7] can be attributed to the core-hole attraction (core exciton), which is consistent with the discussion reported by Ahuja *et al.*[25] Mele *et al.*[26] reported that such discrepancies between the single-particle DOS and the measured core absorption spectra might come from the strong interaction between the final-state electrons with the core-hole left behind, which is supported by Wessely *et al.*[27] This argument is contradicted by Weng *et al.*[28] They concluded that many-body effects are less important for explaining the XAS results for graphite and diamond. We did not discuss the exciton picture in this paper. However, such a discussion does not change the polarization dependence of the XAS spectra of graphene. In the high-energy region, a localized peak at 302.7 eV (solid line E) is observed in Fig. 6(b), which is calculated by the tight-binding model. The corresponding experimental peak in Fig. 6(a) is observed at 303.5 eV, which is identified as a σ symmetry peak (solid line E). Even though the peak positions are not exactly the same, the XAS peak appears at 302.7 eV in the calculated spectra, and the peak at 303.5 eV can be identified as the σ_3 peak, which is consistent with the JDOS data. The calculated peak (solid line E) in the calculated XAS spectra in Fig. 6(b) appears to be associated with localized states because an atomic orbital is used to calculate the absorption matrix element. Between 297.0 and 300.7 eV, no XAS intensity is found in Fig. 6(b) because of the absence of any DOS in this region. On the other hand, in the high-energy region of the experimental XAS spectra in Fig. 6(a), a wavy nature appears and then it is smoothly decreasing as a function of energy, which is like a free-electron DOS and a discussion of these phenomena is not covered by the present tight-binding calculation. In spite of the wavy nature in the high-energy region of the experimental XAS results, a weak peak is visible around 302.5 eV [solid line E) in Fig. 6(a), which is identified as a σ_3^* peak. A calculation using a plane-wave expansion is needed for describing these energy regions, which will be done in a future work.

IV. CONCLUSION

In conclusion, we have calculated the x-ray absorption spectra of graphene using the tight-binding method within the dipole approximation. In the case of the 1s to π^* transition, the dipole vector is directed in the z direction, that is, perpendicular to the graphene plane, while in the 1s to σ^* transition, the dipole vector is directed along the graphene plane. Such different orientations of the dipole vectors, depending on the final-state symmetry, give rise to a polarization dependence of the x-ray absorption spectra of graphene, which is different for the 1s-π^* and the 1s-σ^* transitions. The x-ray absorption intensity is proportional to the square of the absorption matrix element, which corresponds to the inner product of the dipole vector and the polarization vector. Due to the square term of the matrix element, the x-ray absorption intensity for the 1s to π^* (σ^*) transition is linearly proportional to $\sin^2\alpha$ ($\cos^2\alpha$). The present calculation could directly apply to XAS measurements for graphene ribbons and bilayer graphene, etc., since the atomic matrix element should not be changed for these cases.

ACKNOWLEDGMENTS

M.T.C. was supported by a Monbukagakusho scholarship. R.S. acknowledges MEXT (Grant No. 20241023). M.S.D. acknowledges NSF-DMR 10-04147. We like to thank M. Kiguchi of the Tokyo Institute of Technology (TIT) for sharing his experimental reports before publication.

[1]R. Saito, G. Dresselhaus, and M. S. Dresselhaus, *Physical Properties of Carbon Nanotubes* (Imperial College Press, London, 1998).
[2]P. R. Wallace, Phys. Rev. **71**, 622 (1947).
[3]K. S. Novoselov, A. K. Geim, S. V. Morozov, D. Jiang, Y. Zhang, S. V. Dubonos, I. V. Grigorieva, and A. A. Firsov, Science **306**, 666 (2004).
[4]O. V. Yazyev and M. I. Katsnelson, Phys. Rev. Lett. **100**, 047209 (2008).
[5]F. Bonaccorso, Z. Sun, T. Hasan, and A. C. Ferrari, Nat. Photon.**4**, 611 (2010).
[6]P. Castrucci, M. Scarselli, M. D. Crescenzi, M. A. E. Khakani, and F. Rosei, Nanoscale **2**, 1611 (2010).
[7]R. A. Rosenberg, P. J. Love, and V. Rehn, Phys. Rev. B **33**, 4034 (1986).
[8]D. A. Fischer, R. M. Wentzcovitch, R. G. Carr, A. Continenza, and A. J. Freeman, Phys. Rev. B **44**, 1427 (1991).

[9]P. E. Batson, Phys. Rev. B **48**, 2608 (1993).
[10]P. Skytt, P. Glans, D. C. Mancini, J. H. Guo, N. Wassdahl, J. Nordgren, and Y. Ma, Phys. Rev. B **50**, 10457 (1994).
[11]S. Banerjee, T. Hemraj-Benny, S. Sambasivan, D. A. Fischer, J. A. Misewich, and S. S. Wong, J. Phys. Chem. B **109**, 8489 (2005).
[12]P. A. Brühwiler, A. J. Maxwell, C. Puglia, A. Nilsson, S. Andersson, and N. Mårtensson, Phys. Rev. Lett. **74**, 614 (1995).
[13]Y. Ma, P. Skytt, N. Wassdahl, P. Glans, D. C. Mancini, J. Guo, and J. Nordgren, Phys. Rev. Lett. **71**, 3725 (1993).
[14]D. Pacilé, M. Papagno, A. Fraile Rodríguez, M. Grioni, L. Papagno, Ç. Ö. Girit, J. C. Meyer, G. E. Begtrup, and A. Zettl, Phys. Rev. Lett. **101**, 066806 (2008).
[15]S. Y. Zhou, Ç. Ö. Girit, A. Scholl, C. J. Jozwiak, D. A. Siegel, P. Yu, J. T. Robinson, F. Wang, A. Zettl, and A. Lanzara, Phys. Rev. B **80**, 121409 (2009).
[16]M. Papagno, A. Fraile Rodríguez, Ç. Ö. Girit, J. C. Meyer, A. Zettl, and D. Pacilé, Chem. Phys. Lett. **475**, 269 (2009).
[17]B. J. Schultz, C. J. Patridge, V. Lee, C. Jaye, P. S. Lysaght, C. Smith, J. Barnett, D. A. Fischer, D. Prendergast, and S. Banerjee, Nat. Commun.**2**, 372 (2011).
[18]H. K. Jeong, H. J. Noh, J. Y. Kim, L. Colakerol, P. A. Glans, M. H. Jin, K. E. Smith, and Y. H. Lee, Phys. Rev. Lett. **102**, 099701 (2009).
[19]W. Hua, B. Gao, S. Li, H. Ågren, and Y. Luo, Phys. Rev. B **82**, 155433 (2010).
[20]M. Kiguchi, K. Takai, V. L. Joseph Joly, T. Enoki, R. Sumii, and K. Amemiya, Phys. Rev. B **84**, 045421 (2011).
[21]V. L. Joseph Joly, M. Kiguchi, S. J. Hao, K. Takai, T. Enoki, R. Sumii, K. Amemiya, H. Muramatsu, T. Hayashi, Y. A. Kim, M. Endo, J. Campos-Delgado, F. López-Urías, A. Botello-Méndez, H. Terrones, M. Terrones, and M. S. Dresselhaus, Phys. Rev. B **81**, 245428 (2010).
[22]A. Grüneis, R. Saito, Ge. G. Samsonidze, T. Kimura, M. A. Pimenta, A. Jorio, A. G. Souza Filho, G. Dresselhaus, and M. S. Dresselhaus, Phys. Rev. B **67**, 165402 (2003).
[23]R. Saito and T. Kimura, Phys. Rev. B **46**, 1423 (1992).
[24]J. C. Slater, T. M. Wilson, and J. H. Wood, Phys. Rev. **179**, 28 (1969).
[25]R. Ahuja, P. A. Brühwiler, J. M. Wills, B. Johansson, N. Mårtensson, and O. Eriksson, Phys. Rev. B **54**, 14396 (1996).
[26]E. J. Mele and J. J. Ritsko, Phys. Rev. Lett. **43**, 68 (1979).
[27]O. Wessely, M. I. Katsnelson, and O. Eriksson, Phys. Rev. Lett. **94**, 167401 (2005).
[28]X. Weng, P. Rez, and H. Ma, Phys. Rev. B **40**, 4175 (1989).